

¹ ARTICLE TEMPLATE

² **An Application of Spatio-temporal Modeling to Finite Population**
³ **Abundance Prediction**

⁴ Matt Higham^a, Michael Dumelle^b, Carly Hammond^c, Jay Ver Hoef^d, Jeff Wells^c

⁵ ^aSt. Lawrence University Department of Mathematics, Computer Science, and Statistics

⁶ Canton, NY 13617; ^bUnited States Environmental Protection Agency Corvallis, OR 97333;

⁷ ^cAlaska Department of Fish and Game Fairbanks, AK 99701; ^dMarine Mammal Laboratory,

⁸ Alaska Fisheries Science Center, National Oceanic and Atmospheric Administration Seattle,

⁹ Washington 98115

¹⁰ **ARTICLE HISTORY**

¹¹ Compiled January 31, 2023

¹² **ABSTRACT**

¹³ Finite population prediction with spatio-temporal modeling can be used to predict
¹⁴ a quantity of a finite resource from a sample of data collected over both spatial
¹⁵ indices and temporal indices. We develop a spatio-temporal finite population block
¹⁶ kriging (st-FPBK) predictor that incorporates an appropriate variance reduction
¹⁷ for sampling from a finite population. Through an application to moose surveys in
¹⁸ the Tok region of Alaska, we show that the predictor has a substantially smaller
¹⁹ standard error compared to a predictor from the purely spatial model that is cur-
²⁰ rently used to analyze moose surveys in the region. A separate simulation study
²¹ shows that the spatio-temporal predictor is unbiased and that prediction intervals
²² from the st-FPBK predictor attain appropriate coverage. For ecological monitoring
²³ surveys completed with some regularity through time, use of st-FPBK could im-
²⁴ prove precision. Therefore, we also give an R package that ecologists and resource
²⁵ managers could use to incorporate data from past surveys in predicting a quantity
²⁶ from a current survey.

²⁷ **KEYWORDS**

²⁸ spatial; temporal; kriging; total; resource monitoring

²⁹ **1. Introduction**

³⁰ **1.1. Background**

³¹ Spatio-temporal data is indexed by both a spatial index, which we will refer to as
³² a “site,” and by a temporal index, which we will refer to as a “time point.” Com-
³³ mon examples of spatio-temporal data include infections from a disease in a coun-
³⁴ try or region collected over a time period (e.g. Martínez-Beneito, López-Quilez, and
³⁵ Botella-Rocamora 2008; Sahu and Böhning 2022) or climate variables that are recorded
³⁶ through time at multiple locations (Lemos and Sansó 2009).

³⁷ Models for spatio-temporal data have applications in a wide variety of scientific
³⁸ fields (see Wikle, Zammit-Mangion, and Cressie 2019, for many examples). One such

CONTACT Matt Higham. Email: mhigham@stlawu.edu, Michael Dumelle. Email: Dumelle.Michael@epa.gov, Carly Hammond. Email: carly.hammond@alaska.gov, Jay Ver Hoef. Email: jay.verhoef@noaa.gov, Jeff Wells. Email: jeff.wells@alaska.gov

39 application is ecological monitoring of a particular resource, such as animal or plant
40 abundance, rainfall, concentration of a compound in soil samples, etc.

41 In ecological monitoring, we are often interested in prediction of a total or a mean
42 of a particular variable in a finite region in the most recent time point. Ver Hoef (2008)
43 developed Finite Population Block Kriging (FPBK) to predict a linear function of the
44 realized values of a response variable measured at one particular time point in a finite
45 number of sampling units, incorporating a finite population correction to the variance
46 of the predictor. Typically, the linear function is either a mean or a total of the realized
47 values of the response.

48 **1.2. Motivating Example**

49 To motivate the development of the predictor in Section 2, we consider moose surveys,
50 which are performed annually in many regions of Alaska and western Canada. The
51 most common goal of these surveys is to predict moose abundance, the total number
52 of moose, in the region in order to inform harvest regulations (Kellie, Colson, and
53 Reynolds 2019). Because of time and money constraints, only some spatial indices, or
54 sites, in the region of interest are selected to be in the survey at a particular time point.
55 Biologists fly to these selected sites, count the number of moose, and then use FPKB to
56 find a prediction for the finite abundance for that year. These surveys are historically
57 analyzed with software developed by DeLong (2006), which calculates the “GeoSpatial
58 Population Estimator” (GSPE) for a given survey. The GSPE is an application of the
59 FPKB predictor developed by Ver Hoef (2008).

60 Though many of these surveys are annual, most are analyzed completely independently
61 of surveys from previous years (e.g. Gasaway et al. 1986; Kellie and DeLong
62 2006; Boertje et al. 2009; Peters et al. 2014). For example, a model for a survey con-
63 ducted in the year 2019 constructs a prediction for total abundance only from counts
64 on sites that were sampled in that year. However, using counts from previous years
65 in a model that incorporates both spatial and temporal (spatio-temporal) correlation
66 while also using a finite population correction factor based on the proportion of sites
67 surveyed in the most recent year could result in a prediction for the realized total that
68 is more precise than predictions from a purely spatial model.

69 The rest of this paper is organized as follows. In Section 2, we couple spatio-
70 temporal modeling with finite population prediction to develop the Best-Linear-
71 Unbiased-Predictor (BLUP) and its prediction variance for any linear function of a
72 general response variable, including the total abundance across all sites at a particular
73 time point. We call this predictor the st-FPKB (spatio-temporal Finite Population
74 Block Kriging) predictor. In Section 3, we apply the st-FPKB to a moose data set in
75 the Tok region of Alaska. In Section 4, we conduct a simulation study to examine the
76 properties of the st-FPKB predictor and compare its performance to a predictor from
77 a purely spatial model and a simple random sample design-based estimator. Finally,
78 in Section 5, we offer additional thoughts on the application and simulation, and we
79 give directions for future research.

80 **2. Methods**

81 We now give details on the development of the spatio-temporal model and subsequently
82 use this model to develop a finite population correction factor to give a Best-Linear-
83 Unbiased-Predictor (BLUP) and its prediction variance for any linear function of the

84 response vector.

85 2.1. Spatio-temporal Model

86 Let $Y(\mathbf{s}_i, t_j)$, $i = 1, 2, \dots, n_s$ and $j = 1, 2, \dots, n_t$, be a random variable indexed by
 87 a spatial site and a time point, where the vector \mathbf{s}_i contains the coordinates for the
 88 i^{th} spatial site, n_s is the number of unique sites, t_j is the time index for the j^{th} time
 89 point, and n_t is the number of unique time points. If each site is represented at every
 90 time point, a vector of the $Y(\mathbf{s}_i, t_j)$, denoted $\mathbf{y}(\mathbf{s}_i, t_j)$, has length $n_s \cdot n_t \equiv N$. Then, a
 91 spatio-temporal model for $\mathbf{y}(\mathbf{s}_i, t_j)$ is

$$92 \quad \mathbf{y}(\mathbf{s}_i, t_j) = \mathbf{X}\boldsymbol{\beta} + \boldsymbol{\epsilon}(\mathbf{s}_i, t_j), \quad (1)$$

92 where \mathbf{X} is a design matrix for the fixed effects and $\boldsymbol{\beta}$ is a parameter vector of fixed
 93 effects. As in Dumelle et al. (2021), we can decompose the error vector $\boldsymbol{\epsilon}(\mathbf{s}_i, t_j)$ into
 94 spatial, temporal, and spatio-temporal components, each of which will be explained
 95 in detail in the subsequent paragraphs:

$$96 \quad \boldsymbol{\epsilon}(\mathbf{s}_i, t_j) = \mathbf{Z}_s\boldsymbol{\delta} + \mathbf{Z}_s\boldsymbol{\gamma} + \mathbf{Z}_t\boldsymbol{\tau} + \mathbf{Z}_t\boldsymbol{\eta} + \boldsymbol{\omega} + \boldsymbol{\nu}. \quad (2)$$

96 In the spatial component of equation 2 ($\mathbf{Z}_s\boldsymbol{\delta} + \mathbf{Z}_s\boldsymbol{\gamma}$), the matrix \mathbf{Z}_s is an $N \times n_s$
 97 matrix of 0's and 1's, where the values in a row corresponding to a data point at
 98 site \mathbf{s}_i are 1 in the i^{th} column and 0 in all other columns. $\boldsymbol{\delta}$ is a random vector with
 99 mean $\mathbf{0}$ and covariance $\text{cov}(\boldsymbol{\delta}) = \sigma_\delta^2 \mathbf{R}_s$, where \mathbf{R}_s is an $n_s \times n_s$ spatial correlation
 100 matrix and σ_δ^2 is called the spatial dependent error variance (or spatial partial sill).
 101 The random vector $\boldsymbol{\gamma}$ also has mean $\mathbf{0}$ but has covariance $\text{cov}(\boldsymbol{\gamma}) = \sigma_\gamma^2 \mathbf{I}_s$, where \mathbf{I}_s is
 102 the $n_s \times n_s$ identity matrix and σ_γ^2 is called the spatial independent error variance (or
 103 spatial nugget).

104 In the temporal component of equation 2 ($\mathbf{Z}_t\boldsymbol{\tau} + \mathbf{Z}_t\boldsymbol{\eta}$), \mathbf{Z}_t is an $N \times n_t$ matrix of
 105 0's and 1's, where the values in a row corresponding to a data point at time point t_j
 106 are 1 in the j^{th} column and 0 in all other columns. $\boldsymbol{\tau}$ is a random vector with mean
 107 $\mathbf{0}$ and covariance $\text{cov}(\boldsymbol{\tau}) = \sigma_\tau^2 \mathbf{R}_t$, where \mathbf{R}_t is an $n_t \times n_t$ temporal correlation matrix
 108 and σ_τ^2 is called the temporal dependent error variance (or temporal partial sill). $\boldsymbol{\eta}$ is
 109 also a random vector with mean $\mathbf{0}$ but has covariance $\text{cov}(\boldsymbol{\eta}) = \sigma_\eta^2 \mathbf{I}_t$, where \mathbf{I}_t is the
 110 $n_t \times n_t$ identity matrix and σ_η^2 is called the temporal independent error variance (or
 111 temporal nugget).

112 In the spatio-temporal component of equation 2 ($\boldsymbol{\omega} + \boldsymbol{\nu}$), $\boldsymbol{\omega}$ is a random vector
 113 with mean $\mathbf{0}$ and covariance $\text{cov}(\boldsymbol{\omega}) = \sigma_\omega^2 \mathbf{R}_{st}$, where \mathbf{R}_{st} is an $N \times N$ spatio-temporal
 114 correlation matrix and σ_ω^2 is sometimes called the spatio-temporal dependent error
 115 variance (or spatio-temporal partial sill). $\boldsymbol{\nu}$ is also a random vector with mean $\mathbf{0}$ but
 116 has covariance $\text{cov}(\boldsymbol{\nu}) = \sigma_\nu^2 \mathbf{I}_{st}$, where \mathbf{I}_{st} is the $N \times N$ identity matrix and σ_ν^2 is
 117 sometimes called the spatio-temporal independent error variance (or spatio-temporal
 118 nugget).

Though there are a few types of models for the errors that can be built from 2 by
 setting certain error variances to 0 (e.g. a sum-with-error model sets $\sigma_\omega^2 = 0$) and/or
 by allowing \mathbf{R}_{st} to take certain forms, we focus only on the product-sum model. In a
 common formulation of the product-sum model, \mathbf{R}_{st} is

$$119 \quad \mathbf{R}_{st} \equiv \mathbf{Z}_s \mathbf{R}_s \mathbf{Z}'_s \odot \mathbf{Z}_t \mathbf{R}_t \mathbf{Z}'_t,$$

119 where \odot is the Hadamard product operator. \mathbf{R}_s can be parameterized in different
 120 ways, but one common assumption is to assume the covariance function generating
 121 \mathbf{R}_s is second-order stationary (ie. the covariance between two data points is a function
 122 only of the separation vector between two sites) and isotropic (ie. the covariance is a
 123 function of the distance only and does not depend on the direction of the separation
 124 vector). For example, the exponential covariance function is defined as follows. For
 125 observations at sites i and i' at $h_{ii'}$ distance apart, row i and column i' of \mathbf{R}_s is equal
 126 to

$$\exp(-h_{ii'}/\phi), \quad (3)$$

127 where $\exp(x)$ is equivalent to e^x and ϕ is a spatial range parameter controlling the
 128 decay rate of the covariance as distance between two sites increases (Cressie 2015).

129 Similarly, one common assumption when parameterizing \mathbf{R}_t is to assume the covari-
 130 ance function generating \mathbf{R}_t is second-order stationary (ie. the covariance is a function
 131 only of the temporal distance). For example, the exponential covariance function is
 132 defined as follows. For observations at time points j and j' at $m_{jj'}$ units apart, row j
 133 and column j' of \mathbf{R}_t is equal to

$$\exp(-m_{jj'}/\rho), \quad (4)$$

134 where ρ is a temporal range parameter controlling the decay rate of the covariance as
 135 time units between two data points increases. Note that the exponential form of \mathbf{R}_t
 136 is equivalent to an AR(1) time series model if the time points are equally spaced and
 137 the correlation parameter in the AR(1) series is greater than zero (Schabenberger and
 138 Gotway 2017).

139 The product-sum model for $\mathbf{y}(\mathbf{s}_i, t_j)$ is then

$$\mathbf{y}(\mathbf{s}_i, t_j) = \mathbf{X}\boldsymbol{\beta} + \mathbf{Z}_s\boldsymbol{\delta} + \mathbf{Z}_s\boldsymbol{\gamma} + \mathbf{Z}_t\boldsymbol{\tau} + \mathbf{Z}_t\boldsymbol{\eta} + \boldsymbol{\omega} + \boldsymbol{\nu}, \quad (5)$$

140 where $\boldsymbol{\delta}$, $\boldsymbol{\gamma}$, $\boldsymbol{\tau}$, $\boldsymbol{\eta}$, $\boldsymbol{\omega}$, and $\boldsymbol{\nu}$ are mutually independent, $\mathbf{y}(\mathbf{s}_i, t_j)$ has mean $\mathbf{X}\boldsymbol{\beta}$, and
 141 $\mathbf{y}(\mathbf{s}_i, t_j)$ has covariance

$$\text{var}(\mathbf{y}) \equiv \boldsymbol{\Sigma} = \sigma_\delta^2 \mathbf{Z}_s \mathbf{R}_s \mathbf{Z}'_s + \sigma_\gamma^2 \mathbf{Z}_s \mathbf{I}_s \mathbf{Z}'_s + \sigma_\tau^2 \mathbf{Z}_t \mathbf{R}_t \mathbf{Z}'_t + \sigma_\eta^2 \mathbf{Z}_t \mathbf{I}_t \mathbf{Z}'_t + \sigma_\omega^2 \mathbf{R}_{st} + \sigma_\nu^2 \mathbf{I}_{st}. \quad (6)$$

142 There are a few reasons for why we choose to solely focus on the product-sum model.
 143 First, as long as \mathbf{R}_s and \mathbf{R}_t are positive definite and either $\sigma_\omega^2 > 0$ or $\sigma_\nu^2 > 0$, then
 144 the covariance matrix in equation 6 is also positive definite (De Cesare, Myers, and
 145 Posa 2001; De Iaco, Myers, and Posa 2001). Also, the product-sum model is flexible in
 146 its ability to model many kinds of spatial and temporal correlation (De Iaco, Palma,
 147 and Posa 2015). Xu and Shu (2015) claim that the model is the most widely used in
 148 practical applications.

149 2.2. Finite Population Block Kriging

150 The model that we developed in the previous section in equation 5 is for the N -length
 151 vector \mathbf{y} . However, often we do not have the resources to sample or observe every spatial
 152 site during every time point. Therefore, we may have an interest in prediction of the
 153 response values on sites that were not observed, particularly sites in the most recent
 154 time point. Throughout this section, let the subscript o denote data points that were

155 “observed” or sampled, the subscript u denote data points that were “unobserved” or
 156 not sampled, and the subscript a denote “all” data points. Then, we can re-order the
 157 response vector \mathbf{y} so that

$$\mathbf{y}_a \equiv \mathbf{y}_a = [\mathbf{y}'_u, \mathbf{y}'_o]'. \quad (7)$$

158 Our primary goal is to use the model developed for \mathbf{y}_a in equation 5 to find optimal
 159 weights \mathbf{q}' to apply to the observed realizations of \mathbf{y}_o such that $\mathbf{q}'\mathbf{y}_o$ is the Best Linear
 160 Unbiased Predictor (BLUP) for $\mathbf{b}'_a\mathbf{y}_a$, a linear function of \mathbf{y}_a . The N -length vector
 161 \mathbf{b}'_a is, for example, might be a vector of 1’s, in which case we would be predicting the
 162 total response across all sites and all time points.

163 Unbiasedness implies that $E(\mathbf{q}'\mathbf{y}_o) = E(\mathbf{b}'_a\mathbf{y}_a)$ for all β . So, denoting \mathbf{X}_o as the
 164 design matrix for the observed data points and \mathbf{X}_a as the design matrix for all data
 165 points, $\mathbf{q}'\mathbf{X}_o\beta = \mathbf{b}'_a\mathbf{X}_a\beta$ for every β , implying that $\mathbf{q}'\mathbf{X}_o = \mathbf{b}'_a\mathbf{X}_a$. Kriging weights
 166 are then found by finding $\boldsymbol{\lambda}_o$, an $n_o \times 1$ column vector, where n_o is the number of
 167 observed data points, such that

$$E\{(\mathbf{q}'\mathbf{y}_o - \mathbf{b}'_a\mathbf{y}_a)(\mathbf{q}'\mathbf{y}_o - \mathbf{b}'_a\mathbf{y}_a)\} - E\{(\boldsymbol{\lambda}'_o\mathbf{y}_o - \mathbf{b}'_a\mathbf{y}_a)(\boldsymbol{\lambda}'_o\mathbf{y}_o - \mathbf{b}'_a\mathbf{y}_a)\} \quad (8)$$

168 is greater than 0 for all \mathbf{q}' . The prediction equations are

$$\begin{pmatrix} \Sigma_{o,o} & \mathbf{X}_o \\ \mathbf{X}'_o & 0 \end{pmatrix} \begin{pmatrix} \boldsymbol{\lambda} \\ m \end{pmatrix} = \begin{pmatrix} \Sigma_{o,o} & \Sigma_{o,u} \\ \mathbf{X}'_o & \mathbf{X}'_u \end{pmatrix} \begin{pmatrix} \mathbf{b}_o \\ \mathbf{b}_u \end{pmatrix}, \quad (9)$$

169 where again the subscripts o and u denote observed and unobserved data points. For
 170 example, $\Sigma_{o,o}$ denotes the $n_o \times n_o$ submatrix of Σ (from equation 6) corresponding only
 171 to rows and columns of observed data points and $\Sigma_{u,o}$ denotes the $(N-n_o) \times n_o$ subma-
 172 trix of Σ corresponding to rows of data points that were not observed and columns of
 173 data points that were observed. Solving the prediction equations, the optimal predic-
 174 tion weights that are both unbiased and have the smallest possible prediction variance
 175 compared to any other linear predictor are

$$\boldsymbol{\lambda}'_o = \mathbf{b}'_o + \mathbf{b}'_u (\Sigma_{u,o}\Sigma_{o,o}^{-1}) - \mathbf{b}'_u (\Sigma_{u,o}\Sigma_{o,o}^{-1}) \mathbf{X}_o (\mathbf{X}'_o \Sigma_{o,o}^{-1} \mathbf{X}_o)^{-1} \mathbf{X}'_o \Sigma_{o,o}^{-1} + \mathbf{b}'_u \mathbf{X}'_u (\mathbf{X}'_o \Sigma_{o,o}^{-1} \mathbf{X}_o)^{-1} \mathbf{X}_o \Sigma_{o,o}^{-1}. \quad (10)$$

176 The BLUP for $\mathbf{b}'_a\mathbf{y}_a$ is then

$$\widehat{\mathbf{b}'_a\mathbf{y}_a} = \boldsymbol{\lambda}'_o\mathbf{y}_o, \quad (11)$$

which is equivalent to

$$\mathbf{b}'_o\mathbf{y}_o + \mathbf{b}'_u\hat{\mathbf{y}}_u,$$

177 where $\hat{\mathbf{y}}_u = \Sigma_{o,o}\Sigma_{o,o}^{-1}(\tilde{\mathbf{y}}_o - \hat{\mu}_o) + \hat{\mu}_u$ with $\hat{\mu}_o = \mathbf{X}_o\hat{\beta}$ and $\hat{\mu}_u = \mathbf{X}_u\hat{\beta}$. $\hat{\beta}$ is the generalized
 178 least squares estimator $(\mathbf{X}'_o \Sigma_{o,o}^{-1} \mathbf{X}_o)^{-1} \mathbf{X}'_o \Sigma_{o,o}^{-1} \mathbf{y}_o$. We can see then that the predictor
 179 multiplies the observed data \mathbf{y}_o with relevant weights from the \mathbf{b}_o vector, and then
 180 adds in the kriged predictions $\hat{\mathbf{y}}_u$ multiplied with relevant weights from the \mathbf{b}_u vector.

181 The prediction variance of the predictor in equation 11 is

$$E((\boldsymbol{\lambda}'_o\mathbf{y}_o - \mathbf{b}'_a\mathbf{y}_a)(\boldsymbol{\lambda}'_o\mathbf{y}_o - \mathbf{b}'_a\mathbf{y}_a)) = \boldsymbol{\lambda}'_o \Sigma_{o,o} \boldsymbol{\lambda}_o - 2\mathbf{b}'_a \Sigma_{a,o} \boldsymbol{\lambda}_o + \mathbf{b}'_a \Sigma_{a,a} \mathbf{b}_a. \quad (12)$$

182 We call the predictor in equation 11 with Σ in equation 6 the st-FPBK predictor.
 183 A common predictor of interest is the total abundance in the most current time point
 184 of the survey. In this scenario, \mathbf{b}_a is a vector of 1's and 0's, where the k^{th} element of
 185 \mathbf{b}_a is equal to 1 if the k^{th} element of \mathbf{y}_a is from the most recent time point of the
 186 survey and the k^{th} element of \mathbf{b}_a is equal to 0 otherwise. If we order \mathbf{y}_a by (1) the
 187 unobserved data points from past surveys, (2) the unobserved data points from the
 188 current survey, (3) the observed data points from past surveys, and (4) the observed
 189 data points from the current survey, then

$$\mathbf{b}_a = [\mathbf{b}'_{up}, \mathbf{b}'_{uc}, \mathbf{b}'_{op}, \mathbf{b}'_{oc}]' = [\mathbf{0}', \mathbf{1}', \mathbf{0}', \mathbf{1}']', \quad (13)$$

190 where the subscripts *up*, *uc*, *op*, and *oc* denote unobserved sites in past surveys, un-
 191 observed sites in the current survey, observed sites in past surveys, and observed sites
 192 in the current survey, respectively.

193 2.3. *Estimation*

194 In practical applications, the covariance matrix Σ in equation 6 that is partitioned
 195 into the various sub-matrices in equations 11 and 12 needs to be estimated from the
 196 observed data \mathbf{y}_o . The spatio-temporal model in equation 5 does not have any distri-
 197 butional assumptions: we only need to specify the mean and variance of \mathbf{y}_o . Restricted
 198 Maximum Likelihood (REML) can be used to estimate the covariance parameters in
 199 Σ , which we will refer to as $\boldsymbol{\theta} \equiv [\sigma_\delta^2, \sigma_\gamma^2, \phi, \sigma_\tau^2, \sigma_\eta^2, \rho, \sigma_\omega^2, \sigma_\nu^2]'$ (Patterson and Thomp-
 200 son 1971; Harville 1977). Even if \mathbf{y}_a is not multivariate normal, the REML estimator
 201 for the parameter vector $\boldsymbol{\theta}$ is still unbiased (Heyde 1994; Cressie and Lahiri 1993).

202 However, REML estimation can be computationally burdensome, particularly for
 203 large spatio-temporal data sets with many observed sites and time points. Therefore,
 204 we use developments from Dumelle et al. (2021) in the application, the simulations
 205 described in the next section, and the accompanying R package to speed up estimation
 206 of $\boldsymbol{\theta}$.

207 3. Application

208 We now apply the st-FPBK predictor to a moose data set described below. Moose
 209 surveys throughout Alaska and Canada are often conducted annually, making them
 210 good candidates for incorporating temporal correlation.

211 3.1. *Data Description*

212 The Taylor Corridor in the Tok region of Alaska is a popular habitat for moose and
 213 other wildlife. Abundance surveys for moose are performed in the Taylor Corridor of
 214 the Tok region of Alaska annually (Figure 1) so that biologists have an idea about the
 215 abundance of moose each year. In particular, surveys were conducted every year from
 216 2014 through 2020 in every year except 2016, during which there was not sufficient
 217 snow cover to perform a survey. The spatial sampling frame for one particular survey
 218 consists of 381 sites. There are a total of 7 unique time points represented in the data,
 219 including the missing year of 2016. Therefore, N is 2667.

220 In each year of the survey, an aerial team of biologists selects some of the 381 sites

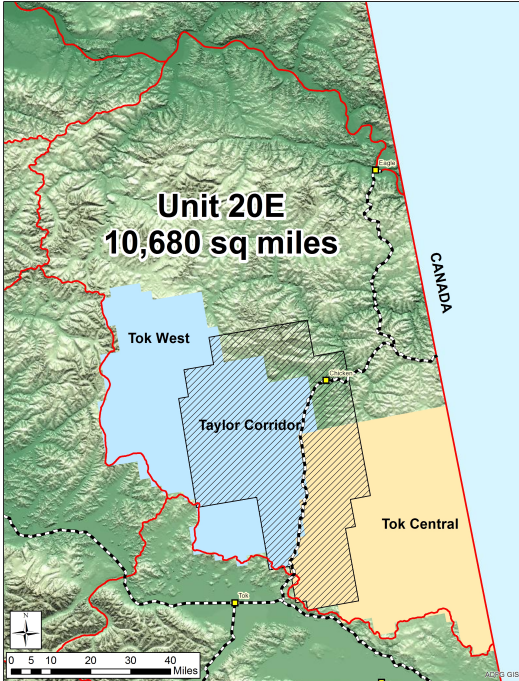


Figure 1. A map of the Taylor Corridor in the Tok region of Alaska.

to survey. The number of sites that are selected varies from a low of 76 in the year 2019 to a high of 90 in the year 2020. Throughout the 7 unique years, some sites are sampled as many as five different times while others are never sampled at all (Figure 2). The number of units sampled throughout all survey years, n , is 487 units.

Before the survey begins in each year, biologists stratify the sites into a "HIGH" stratum composed of 230 sites and a "LOW" stratum composed of 151 sites. The goal of the following analysis is to predict the total abundance of moose across all sites in the year 2020, the most recent year of the survey, using stratum as a covariate in the spatio-temporal model.

3.2. Model Fitting

We fit the product-sum covariance model defined in equation 5 using REML with stratum as a covariate in the design matrix, an exponential spatial correlation structure defined in equation 3, and an exponential temporal correlation structure defined in equation 4. Table 1 gives the estimated parameters from the model fit.

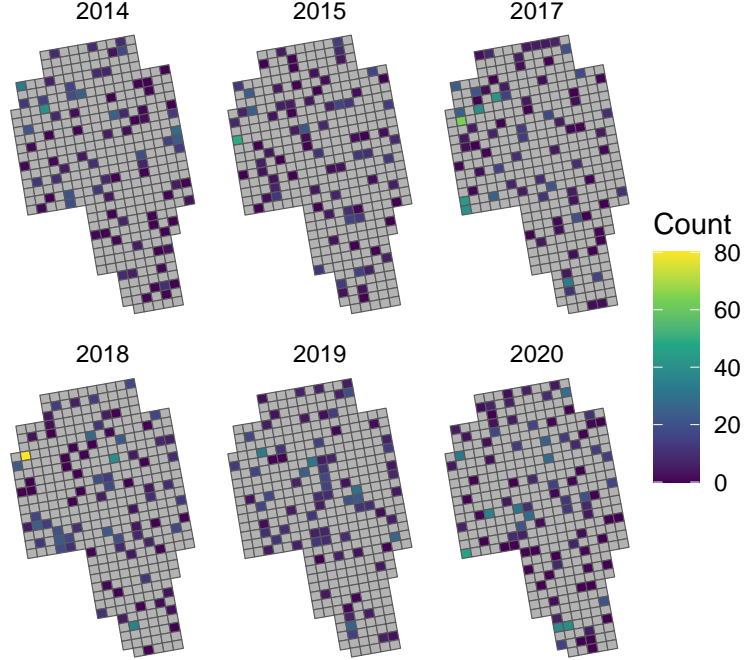


Figure 2. Layout of the spatial sites used to survey moose in the Taylor corridor of the TOK region of Alaska, coloured by moose count. The year 2016 is excluded because no survey was performed in that year. This and all remaining figure graphics are constructed with the `ggplot2` R package (Wickham 2016)

Table 1. Estimated covariance parameters in the model. $\hat{\sigma}_\delta^2$, $\hat{\sigma}_\gamma^2$, and $\hat{\phi}$ are the spatial dependent error variance, independent error variance, and range parameters, respectively. $\hat{\sigma}_\tau^2$, $\hat{\sigma}_\eta^2$, and $\hat{\rho}$ are the temporal dependent error variance, independent error variance, and range parameters, respectively. $\hat{\sigma}_\omega^2$ and $\hat{\sigma}_\nu^2$ are the spatio-temporal dependent error variance and spatio-temporal independent error variance.

Spatial			Temporal			Spatio-temporal	
$\hat{\sigma}_\delta^2$	$\hat{\sigma}_\gamma^2$	$\hat{\phi}$	$\hat{\sigma}_\tau^2$	$\hat{\sigma}_\eta^2$	$\hat{\rho}$	$\hat{\sigma}_\omega^2$	$\hat{\sigma}_\nu^2$
16.91	3.76	4.44	0.88	0.25	2.29	24.01	30.8

To help interpret what some of these fitted covariance parameter estimates mean, we can construct a fitted covariance plot (Figure 3). As the spatial distance between two sites increases (dark colour to light colour), the covariance of two errors decreases to 0, with the $\hat{\phi}$ parameter estimate controlling the rate of decay. In fact, the model estimates the covariance to be nearly 0 when two sites are 20 or more units apart, no matter what the temporal distance is. The covariance between two errors that are six years apart is still estimated to be positive if the two errors come from the same site or from adjacent sites.

The estimated vector of fixed effects, using "HIGH" as the reference group, is $\hat{\beta} = (11.26, -9.76)$. Therefore, the overall mean for sites in the "HIGH" stratum is estimated to be 11.26 moose while the overall mean for sites in the "LOW" stratum is estimated to be 1.5 moose.

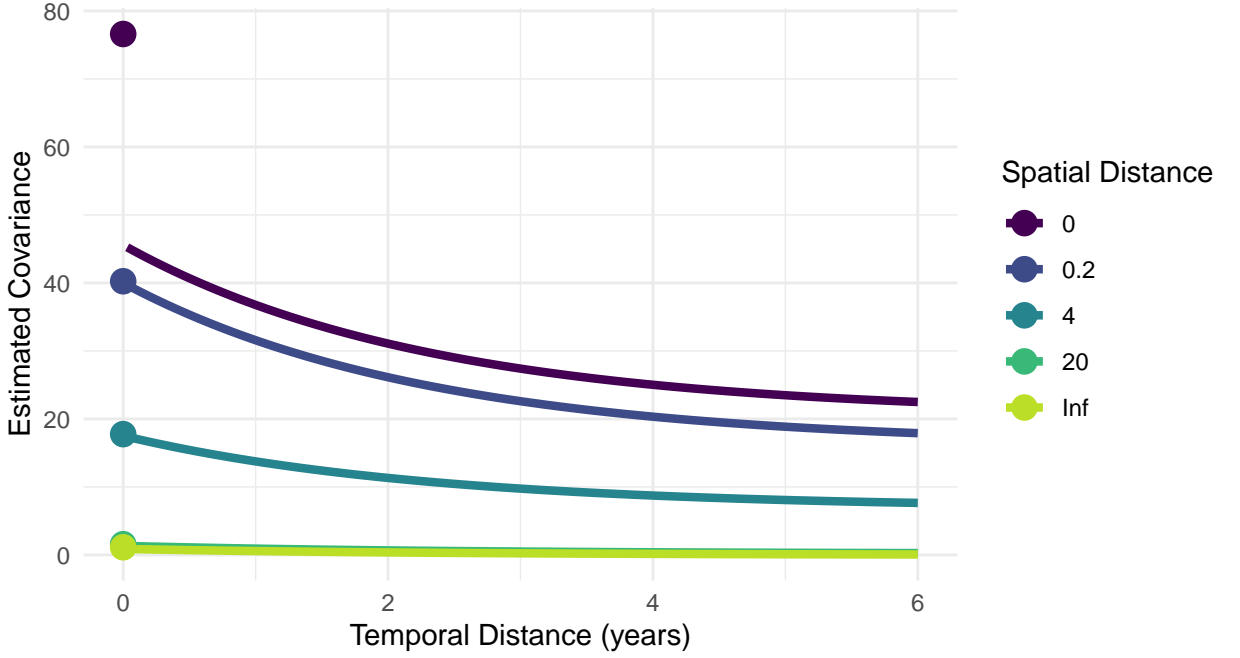


Figure 3. Estimated covariance of the errors from the estimated parameters in a spatio-temporal product-sum model. The centroids of two sites directly adjacent to one another are about 4 units apart.

247 3.3. Prediction

248 We now use the fitted spatio-temporal model with the BLUP from equation 11 and
 249 weights given in equation 13 to predict the total abundance across all sites in the
 250 year 2020, the most recent year of the survey. Plugging in estimates of the covariance
 251 parameters into equations 11 and 12 and letting elements of \mathbf{b}_a be equal to 1 for
 252 data points in 2020 and equal to 0 otherwise, we obtain a prediction of 2874 moose
 253 and a standard error (the square root of the prediction variance) of 234 moose. A 90%
 254 normal-based prediction interval for the total abundance in 2020 is (2489, 3259) moose.
 255 Note that, though the response in this example is a count, a normal-based prediction
 256 interval for the total is still appropriate through an application of the central limit
 257 theorem for dependent data (Smith 1980). Sitewise predictions for sites in 2020 are
 258 given in the map in Figure 4.

259 For comparison, we use the spatial `sptotal` package (Higham et al. 2021) to compute
 260 the spatial FPBK prediction (Ver Hoef 2008) for the total abundance of moose in the
 261 year 2020 with stratum as a covariate. The spatial FPBK predictor is what is currently
 262 implemented in the widely used GSPE software for moose surveys (DeLong 2006).

We also use the stratified random sampling design-based estimator

$$\sum_{i=1}^2 N_i \cdot \bar{y}_i$$

where \bar{y}_i is the sample mean for the observed data in 2020 in the i^{th} stratum and N_i is the total number of sites in 2020 in the i^{th} stratum. The stratified random sampling

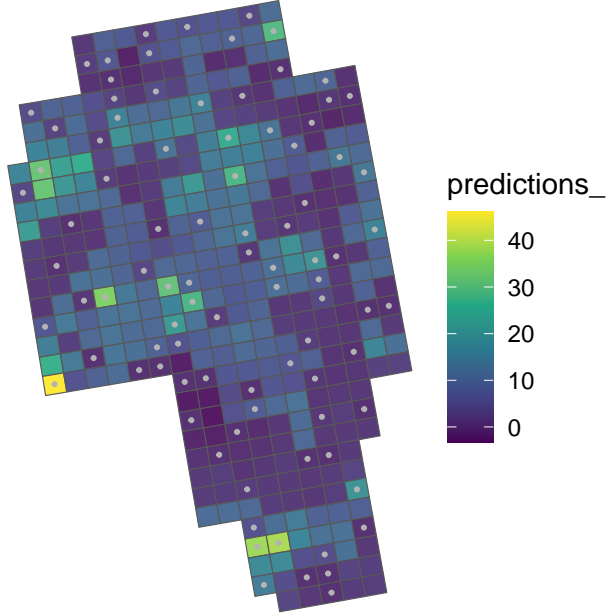


Figure 4. A map of the predictions for the sites in the year 2020. A site with a grey dot in the center means that the site was sampled in 2020.

design-based estimator has a variance for the total abundance of

$$\sum_{i=1}^2 N_i^2 \cdot \left(1 - \frac{n_i}{N_i}\right) \cdot \frac{s_i^2}{n_i},$$

where s_i^2 is the sample variance of the observed data points in 2020 in the i^{th} stratum and n_i is the number of observed data points in 2020 in the i^{th} stratum. Both the purely spatial model fit with `sptotal` and the stratified random sampling design-based estimator use data only from 2020.

For the purely spatial model, the prediction for the total number of moose in 2020 in the region is 2870 moose with a standard error of 319 moose. For the stratified random sampling design-based estimator, the estimated total number of moose in 2020 in the region is 2853 moose with a standard error of 371 moose. While the predictions for the total moose abundance are somewhat similar across the three methods, we see that the spatio-temporal model is most efficient ($SE = 234$ moose compared to 319 moose for the purely spatial model that ignores previous surveys and 371 moose for the stratified random sampling design-based estimator that ignores both previous surveys and spatial correlation in the current survey).

4. Simulation

4.1. Description

To evaluate performance of the st-FPBK predictor, we conduct a simulation study. We simulate a response vector \mathbf{y} of length $N = 1000$ on a 10×10 grid of 100 spatial sites on the unit square ($[0, 1] \times [0, 1]$) and 10 equally-spaced time points in the interval $[0, 1]$, so that each spatial site has a response value at each time point. \mathbf{y} is multivariate

282 normal with mean $\mathbf{0}$ and product-sum covariance matrix Σ defined in equation 6 with
 283 the covariance parameters given in Table 2.

Table 2. Covariance parameters used to simulate data. σ_δ^2 , σ_γ^2 , and ϕ are the spatial dependent error variance, independent error variance, and range parameters, respectively. σ_τ^2 , σ_η^2 , and ρ are the temporal dependent error variance, independent error variance, and range parameters, respectively. σ_ω^2 and σ_ν^2 are the spatio-temporal dependent error variance and spatio-temporal independent error variance.

scenario	Spatial			Temporal			Spatio-temporal	
	σ_δ^2	σ_γ^2	ϕ	σ_τ^2	σ_η^2	ρ	σ_ω^2	σ_ν^2
all-dev	0.5	0.17	0.47	0.5	0.17	0.33	0.50	0.17
t-iev	0	0	0.47	0	1.50	0	0.25	0.25
spt-iev	0	0	0	0	0	0	0	2.00

284 The three scenarios in the table correspond to (1) **all-dev**: a scenario where a
 285 substantial proportion of the overall variance comes from the spatial, temporal, and
 286 spatio-temporal dependent error variance parameters σ_δ^2 , σ_τ^2 , and σ_ω^2 ; (2) **t-iev**: a sce-
 287 nario where there the overall variance is dominated by the temporal independent error
 288 variance parameter, σ_η^2 ; and (3) **spt-iev**: a scenario where all of the variability comes
 289 from σ_ν^2 so that errors are independent regardless of spatial and time indices. In all
 290 scenarios, summing all six variance parameters gives a total variance equal to two
 291 units squared.

292 Both \mathbf{R}_s and \mathbf{R}_t are generated from the exponential correlation function with ϕ
 293 and ρ as the range parameters in equations 3 and 4. The values 0.471 and 0.3333 are
 294 chosen for ϕ and ρ , respectively, so that the effective ranges, 3ϕ and 3ρ , are equal
 295 to the maximum distance between two data points in space ($\sqrt{2} = 1.414$) and the
 296 maximum distance between two data points in time (1). A value of 0 for ϕ (or ρ) sets
 297 the \mathbf{R}_s (or the \mathbf{R}_t) matrix to the identity matrix. Figure 5 shows the model covariance
 298 of the errors used to generate data for the “all-dev” scenario.

299 Each of these three scenarios is replicated for two different sample sizes: $n = 250$
 300 and $n = 500$. A simple random sample of the 1000 total data points is used to select
 301 units to be in the sample.

302 Finally, the simulation experiment is repeated for a skewed response variable. To
 303 create the skewed response variable, a normally-distributed response is simulated ac-
 304 cording to the parameters given in Table 2, except that each of the variance parameters
 305 (not including ϕ and ρ) is divided by 2.89 so that the total variance is equal to 0.6931.
 306 This variable is then exponentiated so that the total variance after exponentiation is
 307 equal to 2. Note that, not only does exponentiation result in a right-skewed response
 308 variable, but exponentiating also allows for an assessment of how the st-FPBK predic-
 309 tor performs when the covariance is mis-specified, as the resulting response variable
 310 is now simulated with an intractable covariance function form that is not used in the
 311 model fitting.

312 Therefore, the simulation study has 12 total settings coming from a $3 \times 2 \times 2$ (scenario
 313 \times sample size \times distribution shape) factorial design. For each setting, we simulate 1000
 314 realizations of the response vector \mathbf{y} . For each realization, we use three methods to
 315 predict the total response for the “most current” time point, which is when the time
 316 index is equal to 1 on the interval $[0, 1]$). We will henceforth call this “total response
 317 for the most current time point quantity” the “current total.”

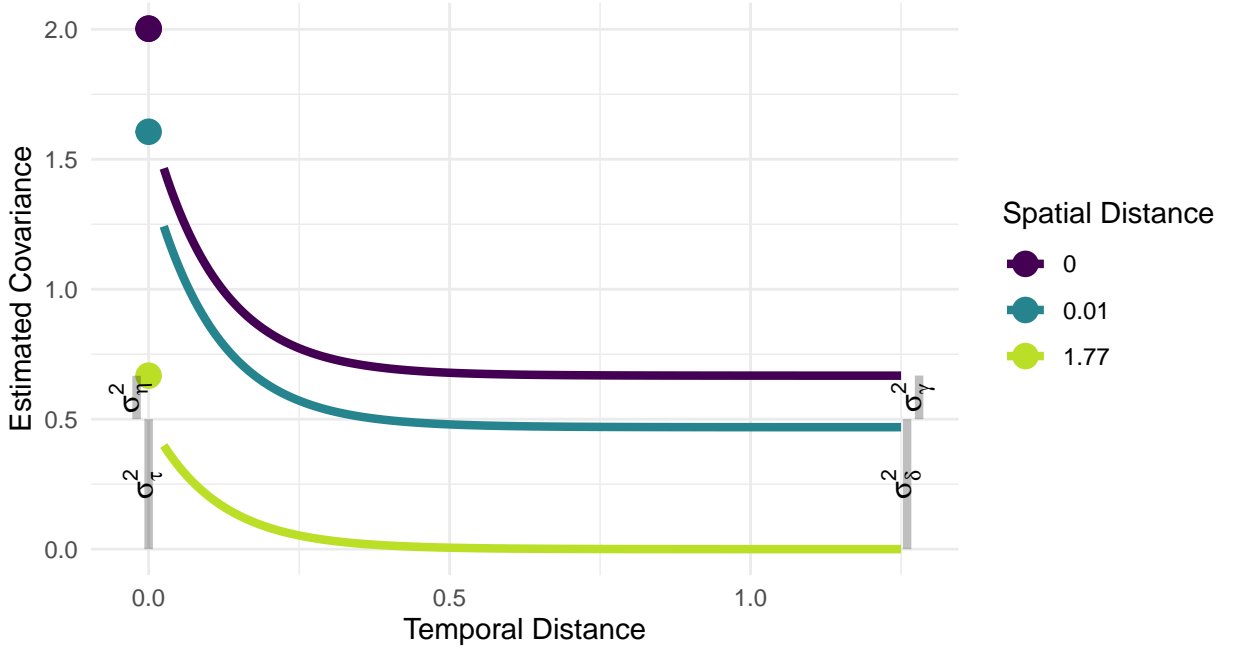


Figure 5. The model covariance used in the simulations for the spatio-temporal scenario. Covariance is approximately 0 for errors from data points that are $\sqrt{2}$ distance units apart in space or 1 distance unit apart in time. The spatial dependent error variance (σ_δ^2), spatial independent error variance (σ_γ^2), temporal dependent error variance (σ_τ^2), and temporal independent error variance (σ_η^2) are shown with grey lines.

318 The first method uses the st-FPBK predictor in equation 11 with the spatio-
 319 temporal model covariance in equation 6. REML estimation with the observed data \mathbf{y}_o
 320 is used to obtain estimates for the covariance parameter vector $\boldsymbol{\theta}$. The second method
 321 is the FPBK spatial model fit with the `sptotal` R package (Higham et al. 2021) that
 322 only uses data from the most current time point.

323 The third method uses a simple random sample (SRS) design-based estimator with
 324 data from the most current time point. The SRS design-based estimator for the total
 325 is $100 \cdot \bar{y}$, where \bar{y} is the sample mean of the response in the most current time point.
 326 The variance of the estimator (Lohr 2021) is $100^2 \cdot \frac{s^2}{n_1} \cdot (1 - \frac{n_1}{100})$, where s^2 is the sample
 327 variance of the response variable in the most current time point and n_1 is the number
 328 of sampled locations in the most current time point.

329 The SRS method gives an estimator, not a predictor, and a corresponding confidence
 330 interval, not a prediction interval, because the SRS design-based estimator treats the
 331 observed data as fixed, not as a random realization from a process (Brus 2021; Dumelle
 332 et al. 2022). However, in the remaining text and tables, we refer to the “current
 333 total” response quantity obtained from the three methods as a “prediction” and to
 334 the corresponding interval as a “prediction interval” to limit unnecessarily verbose
 335 text and tables.

336 For each method, we calculate the root-mean-squared-prediction-error (rMSPE)
 337 as $\frac{1}{1000} \sqrt{\sum_{i=1}^{1000} (T_i - \hat{T}_i)^2}$, where T_i and \hat{T}_i are the realized and predicted current
 338 totals, respectively, in the i^{th} iteration. Bias is recorded as $\frac{1}{1000} \sum_{i=1}^{1000} (T_i - \hat{T}_i)$. We
 339 also create a normal-based 90% prediction interval for the realized current total and
 340 record $\frac{1}{1000} \sum_{i=1}^{1000} I(LB_i < T_i < UB_i)$, where $I(LB_i < T_i < UB_i)$ is an indicator
 341 variable that is equal to 1 if the realized total in iteration i , T_i , is between the lower

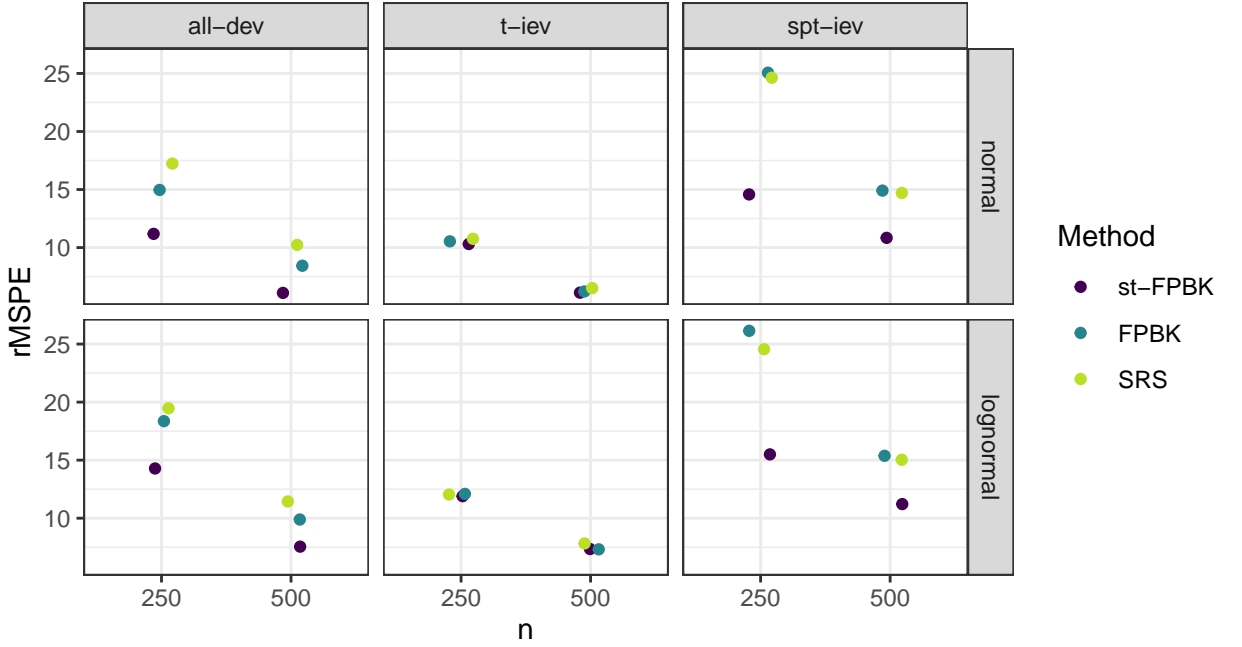


Figure 6. root-mean-squared-prediction-error (rMSPE) for all simulation settings. The st-FPBK predictor has the smallest rMSPE in all settings tested, though it is similar to the rMSPE of the other two methods in the t-iev scenario.

342 bound, LB_i , and the upper bound, UB_i , of the i^{th} prediction interval.

343 4.2. Results

344 Tables 4, 5, and 6 in Section 6 give the rMSPE, bias, and interval coverage of the three
 345 methods in all 12 simulation settings. In Figure 6, we see that the st-FPBK predictor
 346 outperforms both the purely spatial FPKB predictor and the simple random sam-
 347 ple design-based estimator in all of the “all-dev” and “spt-iev” scenarios. In general,
 348 rMSPE improvement is larger for the smaller sample size.

349 We see little gains in rMSPE for the st-FPBK predictor in the “t-iev” scenario.
 350 This setting was chosen to explore how the spatio-temporal model would perform
 351 when most of the variability in the response comes from σ_η^2 , which allows for data
 352 collected in different time points to be uncorrelated, and, for different time points to
 353 have very different realized totals. As expected, the st-FPBK predictor performs no
 354 better than a purely spatial model or the SRS design-based estimator for this scenario;
 355 however, we can also say that the added complexity of the spatio-temporal model is
 356 not detrimental.

357 All methods appear relatively unbiased in all simulation settings: Table 5 shows
 358 that the bias of each method is small compared to the squares of the rMSPE values
 359 given in Table 4.

360 Figure 7 shows the interval coverage for the normal-based prediction intervals
 361 (Smith 1980), where the nominal level is 0.90. We see that the st-FPBK predictor
 362 for the current total has approximate 90% coverage in all settings tested. The spa-
 363 tial model and the SRS design-based estimator have lower than nominal coverage in
 364 some settings because of the small sample size used (recall that the $n = 250$ observed
 365 samples span 10 unique time points so that, on average, the spatial model and SRS

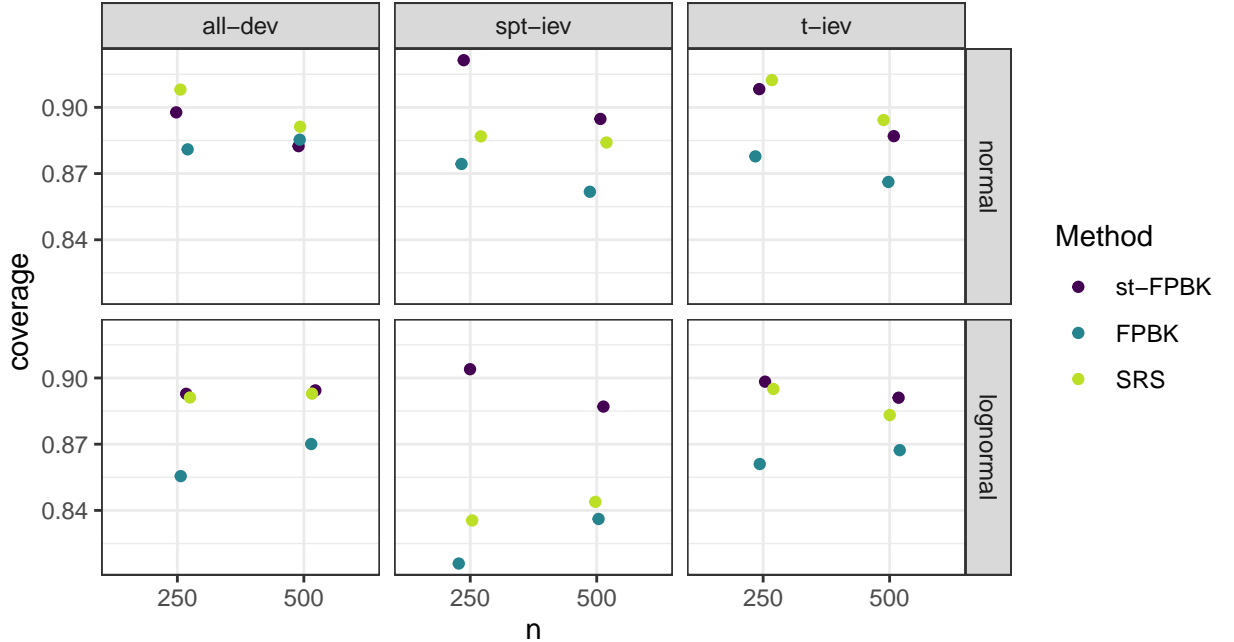


Figure 7. Prediction interval coverage for all simulation settings, where the prediction intervals are normal-based and the nominal level is 0.90. The st-FPBK predictor has close to appropriate coverage in all settings tested.

366 design-based estimator only have 25 observed responses to use in the current time
 367 point).

368 5. Discussion

369 We see in the moose application in Section 3 that there is substantial reduction in
 370 the standard error of the predictor for the total moose abundance in 2020 when in-
 371 corporating data from surveys in previous years. In the simulation study in 4, we find
 372 that the st-FPBK predictor has lower rMSPE than the FPBK predictor from a purely
 373 spatial model and an SRS design-based estimator in many settings. The st-FPBK
 374 predictor is less beneficial when the temporal independent error variance contributes
 375 a large proportion to the overall variance. Additionally, the st-FPBK predictor main-
 376 tains appropriate interval coverage in all settings tested, even when the covariance for
 377 the errors is mis-specified.

378 An additional possible benefit of using the st-FPBK predictor compared to a purely
 379 spatial FPBK predictor is the potential for forecasting abundance before a survey is
 380 completed. For example, in our application, we can refit the model without any of
 381 the observed counts from the 2020 survey and examine the prediction for the total
 382 abundance in the year 2020. Table 3 compares the model with the 2020 data used and
 383 the model without the 2020 data used. We see that, while there is a substantial loss
 384 in precision by excluding the 2020 data (as we would expect), the prediction is not
 385 very different from the prediction with the 2020 data included. And, the prediction
 386 interval might be narrow enough to still be useful to wildlife management. We could
 387 also consider using such an approach if there is a year during which a survey cannot
 388 be completed for logistical reasons. For example, in the Tok region of Alaska, a moose

389 survey was not conducted at all in the year 2016 because there was insufficient snow
390 cover for the survey. The spatio-temporal predictor could still be applied to get a
391 prediction for moose abundance using survey data from previous years.

Table 3. Results from analysis on the Tok moose survey data with the 2020 survey included and excluded. We can see that, even with 2020 data excluded, we can obtain a prediction for moose abundance in 2020, though there is substantial loss in precision.

	Prediction	SE	90% LB	90% UB
2020 Data Included	2874	234	2489	3259
2020 Data Excluded	2757	417	2071	3444

392 We would also like to give our perception of the benefits and drawbacks of our
393 approach with that of Schmidt et al. (2022), who use a hierarchical Bayesian model
394 to predict total abundance, among other quantities of interest. The benefits of our
395 frequentist approach include a faster fitting time, as there is no need to construct and
396 implement the time-consuming Markov chain Monte Carlo sampler. Therefore, our
397 approach is easier to assess in a simulation study, which would be too time-prohibitive
398 for the Bayesian model. Biometricalians could also use simulation with our approach to
399 answer various questions given proposed values of covariance parameters like how much
400 efficiency would drop if a survey was only conducted every other year. Additionally,
401 we argue that our approach is simpler overall for a practitioner to use and could be
402 integrated more readily with the current GSPE software.

403 The Bayesian approach by Schmidt et al. (2022), however, offers features that would
404 be harder to implement in our approach. In general, the model is more flexible, and
405 allows for incorporation of more levels in the Bayesian hierarchical model, including
406 allowing for imperfect detection of animals from a separate detectability survey. Addi-
407 tionally, the Bayesian hierarchical model can use a Poisson or negative binomial model
408 for the counts. Therefore, an appropriate prediction interval for the response on one
409 particular site could be constructed. On the other hand, for our approach, we rely
410 on the central limit theorem for dependent data to form a prediction interval for the
411 total, which would not apply for a prediction interval for the response on just one site.

412 We have developed a finite population block kriging predictor for spatio-temporal
413 data, which adjusts the variance of the predictor to be appropriate for sampling from
414 a finite population. In many settings, the resulting predictor is improved from a pre-
415 dictor with a purely spatial model. Monitoring programs that use regularly scheduled
416 surveys should consider incorporating data from past surveys to improve precision in
417 the predictor for the most current survey.

418 Future work in this area includes developing a frequentist model for which imperfect
419 detection of units through time is incorporated into the predictor or how best to select
420 sites to sample for future surveys given proposed values for the spatio-temporal covari-
421 ance parameters. Additionally, for moose surveys in particular, updating the GSPE
422 software to include analysis for spatio-temporal data could be useful for practitioners.
423 Though we recognize that doing so would be a substantial undertaking, the R package
424 that we provide could be a useful starting point for the integration.

425 **6. Appendix**

Table 4. root-mean-squared-prediction-error (rMSPE) for the st-FPBK predictor, the FPBK predictor, and the SRS estimator for each of the 12 simulation settings. In all settings, the rMSPE for the st-FPBK predictor is approximately equal to or lower than the rMSPE for the other two methods.

Simulation Setting			rMSPE		
scenario	n	Response Type	st-FPBK	FPBK	SRS
spt-iev	250	normal	14.58	25.06	24.64
	250	normal	10.31	10.53	10.76
	250	normal	11.18	14.97	17.23
t-iev	500	normal	10.84	14.91	14.71
	500	normal	6.12	6.22	6.50
	500	normal	6.09	8.43	10.24
all-dev	250	lognormal	15.49	26.14	24.56
	250	lognormal	11.89	12.10	12.05
	250	lognormal	14.28	18.35	19.46
spt-iev	500	lognormal	11.22	15.38	15.04
	500	lognormal	7.34	7.32	7.82
	500	lognormal	7.55	9.89	11.45

Table 5. Bias (Realized Current Total - Predicted Current Total) for the st-FPBK predictor, the FPBK predictor, and the SRS estimator for each of the 12 simulation settings. In all settings, all methods appear fairly unbiased.

Simulation Setting			Bias		
scenario	n	Response Type	st-FPBK	FPBK	SRS
spt-iev	250	normal	0.73	1.38	1.55
	250	normal	0.44	0.39	0.47
	250	normal	0.48	0.27	0.45
t-iev	500	normal	0.46	0.60	0.67
	500	normal	0.15	0.14	0.07
	500	normal	0.04	0.07	0.04
all-dev	250	lognormal	0.36	0.56	1.48
	250	lognormal	0.33	0.22	0.41
	250	lognormal	-0.07	-0.85	-0.49
spt-iev	500	lognormal	0.32	0.29	0.66
	500	lognormal	0.24	0.15	0.08
	500	lognormal	-0.10	-0.39	-0.37

Table 6. Prediction interval coverage for the st-FPBK predictor, the FPBK predictor, and the SRS for each of the 12 simulation settings. All intervals are normal-based and have a nominal coverage level of 0.90.

Simulation Setting			Coverage		
scenario	n	Response Type	st-FPBK	FPBK	SRS
spt-iev	250	normal	0.92	0.87	0.89
	250	normal	0.91	0.88	0.91
	250	normal	0.90	0.88	0.91
t-iev	500	normal	0.90	0.86	0.88
	500	normal	0.89	0.87	0.89
	500	normal	0.88	0.89	0.89
all-dev	250	lognormal	0.90	0.82	0.84
	250	lognormal	0.90	0.86	0.90
	250	lognormal	0.89	0.86	0.89
spt-iev	500	lognormal	0.89	0.84	0.84
	500	lognormal	0.89	0.87	0.88
	500	lognormal	0.89	0.87	0.89

426 References

- 427 Boertje, Rodney D, Mark A Keech, Donald D Young, Kalin A Kellie, and C Tom Seaton.
428 2009. “Managing for elevated yield of moose in interior Alaska.” *The Journal of Wildlife
429 Management* 73 (3): 314–327.
- 430 Brus, Dick J. 2021. “Statistical approaches for spatial sample survey: Persistent misconceptions
431 and new developments.” *European Journal of Soil Science* 72 (2): 686–703.
- 432 Cressie, Noel. 2015. *Statistics for spatial data - revised edition*. John Wiley & Sons.
- 433 Cressie, Noel, and Soumendra Nath Lahiri. 1993. “The asymptotic distribution of REML
434 estimators.” *Journal of multivariate analysis* 45 (2): 217–233.
- 435 De Cesare, Luigi, DE Myers, and D Posa. 2001. “Product-sum covariance for space-time model-
436 ing: an environmental application.” *Environmetrics: The official journal of the International
437 Environmetrics Society* 12 (1): 11–23.
- 438 De Iaco, S, M Palma, and D Posa. 2015. “Spatio-temporal geostatistical modeling for French
439 fertility predictions.” *Spatial Statistics* 14: 546–562.
- 440 De Iaco, Sandra, Donald E Myers, and Donato Posa. 2001. “Space-time analysis using a
441 general product-sum model.” *Statistics & Probability Letters* 52 (1): 21–28.
- 442 DeLong, Robert A. 2006. *Geospatial population estimator software user’s guide*. Alaska De-
443 partment of Fish and Game, Division of Wildlife Conservation.
- 444 Dumelle, Michael, Matt Higham, Jay M Ver Hoef, Anthony R Olsen, and Lisa Madsen. 2022.
445 “A comparison of design-based and model-based approaches for finite population spatial
446 sampling and inference.” *Methods in Ecology and Evolution* 13 (9): 2018–2029.
- 447 Dumelle, Michael, Jay M Ver Hoef, Claudio Fuentes, and Alix Gitelman. 2021. “A linear mixed
448 model formulation for spatio-temporal random processes with computational advances for
449 the product, sum, and product-sum covariance functions.” *Spatial Statistics* 43: 100510.
- 450 Gasaway, William C, Stephen D DuBois, Daniel J Reed, and Samuel J Harbo. 1986. *Estimating
451 moose population parameters from aerial surveys*. Technical Report. University of Alaska.
452 Institute of Arctic Biology.
- 453 Harville, David A. 1977. “Maximum likelihood approaches to variance component estimation

- 454 and to related problems.” *Journal of the American statistical association* 72 (358): 320–338.
- 455 Heyde, CC. 1994. “A quasi-likelihood approach to the REML estimating equations.” *Statistics
& Probability Letters* 21 (5): 381–384.
- 456 Higham, Matt, Jay Ver Hoef, Bryce Frank, and Michael Dumelle. 2021. *sptotal: Predicting
Totals and Weighted Sums from Spatial Data*. R package version 1.0.0, <https://highamm.github.io/sptotal/index.html>.
- 457 Kellie, Kalin A, and Robert A DeLong. 2006. *Geospatial survey operations manual*. Technical
Report. Alaska Department of Fish and Game.
- 458 Kellie, Kalin Ann, Cassidy E Colson, and Joel H Reynolds. 2019. *Challenges to Monitoring
Moose in Alaska*. Alaska Department of Fish and Game, Division of Wildlife Conservation
Juneau
- 459 Lemos, Ricardo T, and Bruno Sansó. 2009. “A spatio-temporal model for mean, anomaly, and
trend fields of North Atlantic sea surface temperature.” *Journal of the American Statistical
Association* 104 (485): 5–18.
- 460 Lohr, Sharon L. 2021. *Sampling: design and analysis*. Chapman and Hall/CRC.
- 461 Martínez-Beneito, Miguel A, Antonio López-Quilez, and Paloma Botella-Rocamora. 2008. “An
autoregressive approach to spatio-temporal disease mapping.” *Statistics in medicine* 27 (15):
2874–2889.
- 462 Patterson, H Desmond, and Robin Thompson. 1971. “Recovery of inter-block information
when block sizes are unequal.” *Biometrika* 58 (3): 545–554.
- 463 Peters, Wibke, Mark Hebblewhite, Kirby G Smith, Shevenell M Webb, Nathan Webb, Mike
Russell, Curtis Stambaugh, and Robert B Anderson. 2014. “Contrasting aerial moose pop-
ulation estimation methods and evaluating sightability in west-central Alberta, Canada.”
Wildlife Society Bulletin 38 (3): 639–649.
- 464 Sahu, Sujit K, and Dankmar Böhning. 2022. “Bayesian spatio-temporal joint disease mapping
of Covid-19 cases and deaths in local authorities of England.” *Spatial Statistics* 49: 100519.
- 465 Schabenberger, Oliver, and Carol A Gotway. 2017. *Statistical methods for spatial data analysis:
Texts in statistical science*. Chapman and Hall/CRC.
- 466 Schmidt, Joshua H, Matthew D Cameron, Kyle Joly, Jordan M Pruszenski, Joel H Reynolds,
and Mathew S Sorum. 2022. “Bayesian spatial modeling of moose count data: increasing
estimator efficiency and exploring ecological hypotheses.” *The Journal of Wildlife Manage-
ment* e22220.
- 467 Smith, Tony E. 1980. “A central limit theorem for spatial samples.” *Geographical Analysis* 12
(4): 299–324.
- 468 Ver Hoef, Jay M. 2008. “Spatial methods for plot-based sampling of wildlife populations.”
Environmental and Ecological Statistics 15 (1): 3–13.
- 469 Wickham, Hadley. 2016. “Data analysis.” In *ggplot2*, 189–201. Springer.
- 470 Wikle, Christopher K, Andrew Zammit-Mangion, and Noel Cressie. 2019. *Spatio-temporal
Statistics with R*. Chapman and Hall/CRC.
- 471 Xu, Jiaqi, and Hong Shu. 2015. “Spatio-temporal kriging based on the product-sum model:
some computational aspects.” *Earth Science Informatics* 8 (3): 639–648.